

Modeling the Resting State of Oxalate Oxidase and Oxalate Decarboxylase Enzymes

Marciela Scarpellini,^{†,‡} Jessica Gätjens,^{†,§} Ola J. Martin,[△] Jeff W. Kampf,[†] Suzanne E. Sherman,^{*,△} and Vincent L. Pecoraro^{*,†}

Willard H. Dow Laboratories, Department of Chemistry, University of Michigan, 930 North University, Ann Arbor, Michigan 48109, and New College of Florida, 5800 Bay Shore Rd., Sarasota, Florida 34243

Received October 2, 2007

In view of the biological and commercial interest in models for Oxalate Decarboxylases (OxDC) and Oxalate Oxidases (OxOx), we have synthesized and characterized three new Mn^{II} complexes (**1–3**) employing N₃O-donor amino-carboxylate ligands (TCMA, 1,4,7-triazacyclononane-*N*-acetic acid; K⁺Pr₂TCMA, potassium 1,4-diisopropyl-1,4,7-triazacyclononane-*N*-acetate; and KBPZG, potassium *N,N*-bis(3,5-dimethylpyrazolyl methyl)glycinate). These complexes were characterized by several techniques including X-ray crystallographic analysis, X-band electron paramagnetic resonance (EPR), electrospray ionization mass spectrometry (ESI-MS), and cyclic voltammetry. The crystal structures of **1** and **3** revealed that both form infinite polymeric chains of Mn^{II} complexes linked by the pendant carboxylate arms of the TCMA⁻ and the BPZG⁻ ligands in a *syn-antipattern*. Complex **2** crystallizes as a mononuclear Mn^{II} cation, six-coordinate in a distorted octahedral geometry. Although complexes **1** and **3** crystallize as polymeric chains, all compounds present the same N₃O-donor set atoms around the metal center as observed in the crystallographically characterized OxDC and OxOx. Moreover, complex **2** also contains two water molecules coordinated to the Mn center as observed in the active site of OxDC and OxOx. ESI-MS spectrometry, combined with EPR, were useful techniques to establish that complexes **1–3** are present as mononuclear Mn^{II} species in solution. Finally, complexes **1–3** are able to model the resting state active sites, with special attention focused on complex **2** which provides the first exact first coordination sphere ligand structural model for the resting states of both OxDC and OxOx.

Introduction

Oxalate is a toxic compound for humans primarily obtained through a diet rich in plants.¹ Since oxalate-degrading enzymes are absent in humans, the ingestion of large amounts of this ion can cause several disorders including kidney stones, cardiological diseases, and renal

failure.^{2,3} In a number of higher plants,⁴ bacteria,⁵ and fungi,⁶ oxalate metabolism is carried out by three groups of enzymes classified according to the type of the catalyzed reaction: (i) Oxalate Decarboxylases (OxDC), responsible for the conversion of oxalate to formate and CO₂; (ii) Oxalate Oxidases (OxOx), mediating the oxygen-dependent oxidation of oxalate to CO₂ and H₂O₂; and (iii) Oxalyl-CoA Decarboxylases, catalyzing the thiamin dependent conversion of oxalyl-CoA to formyl-CoA and CO₂.⁷

* To whom correspondence should be addressed. E-mail: vlpec@umich.edu (V.L.P.), sherman@ncf.edu (S.E.S.). Phone: +1-734-7611519(V.L.P.), +1-941-487-4376(S.E.S.). Fax: +1-734-6474865 (V.L.P.), +1-941-487-4396 (S.E.S.).

[†] University of Michigan.

[‡] Current address: Departamento de Química Inorgânica, Instituto de Química, Universidade Federal do Rio de Janeiro, 21945-970, Rio de Janeiro, RJ, Brazil.

[§] Current address: University of Vienna, Institute of Inorganic Chemistry, Währinger Str. 42, A-1090 Vienna, Austria.

[△] New College of Florida.

(1) (a) Williams, H. E.; Wandzilak, T. R. *J. Urol.* **1989**, *141*, 742–749. (b) Kesarwani, M.; Azam, M.; Natarajan, K.; Mehta, A.; Datta, A. *J. Biol. Chem.* **2000**, *275*, 7230–7238.

(2) Hamano, S.; Nakatsu, H.; Suzuki, N.; Tomioka, S.; Tanaka, M.; Murakami, S. *Int. J. Urol.* **2005**, *12*, 859–863.

(3) (a) Curhan, G. C. *Miner. Electrolyte Metab.* **1997**, *23*, 261–264. (b) Williams, H. E.; Wandzilak, T. R. *J. Urol.* **1989**, *141*, 742–747.

(4) Kotsira, V. P.; Clonis, Y. D. *Arch. Biochem. Biophys.* **1997**, *340*, 239–249.

(5) Quayle, J. R. *Biochem. J.* **1963**, *87*, 368–373.

(6) Shimazono, H. *J. Biochem.* **1955**, *42*, 321–340.

(7) Svedrueić, D.; Jönsson, S.; Toyota, C. G.; Reinhardt, L. A.; Ricagno, S.; Lindqvist, Y.; Richards, N. G. J. *Arch. Biochem. Biophys.* **2005**, *433*, 176–192.

Spectroscopic studies of OxDC⁸ and OxOx^{9,10} revealed that both are manganese-dependent enzymes. Electron paramagnetic resonance (EPR) data at low temperature indicate the presence of Mn^{II} ions, with a strong six-line ⁵⁵Mn ($I = 5/2$) multiplet at $g = 2$, displaying nuclear hyperfine splitting ($A = 95$ G).¹¹ Studies employing the recombinant barley OxOx showed that this signal is strongly influenced by the addition of oxalate and bulky anions, demonstrating the interaction between the Mn-binding center and the substrate.¹¹

A high similarity between the Mn-binding sites of these enzymes was revealed by X-ray crystallographic analyses of OxDC¹² and OxOx,¹³ in which a Mn^{II} ion is observed in a distorted octahedral geometry. Figure 1A presents the Mn-binding site of the OxOx from *Hordeum vulgare* (barley, pdb 1FI2),¹³ where the Mn^{II} is coordinated by three histidines (His88, His90, and His137), one glutamate (Glu95), and two water molecules.

For domain I of the OxDC from *Bacillus subtilis* (Figure 1B), in addition to three histidines (His95, His97 and His140), one glutamate (Glu101), and one water molecule, a formate anion was modeled into the coordination sphere of Mn^{II} suggesting this domain acts as the catalytic center.¹²

In spite of the successful structural characterization of both OxDC and OxOx, details about the catalytic mechanism by which these enzymes degrade oxalate remain unclear and have been the subject of research in the past few years.^{10,15–22} It has been proposed^{8,9,17} that during the catalytic cycle the Mn^{II} center interacts with the oxalate anion and a dioxygen molecule through the displacement of the two coordinated water molecules. Catalysis is then proposed to require a Mn^{II} → Mn^{III} oxidation process.¹⁷ Apparently, two different binding modes of the substrate are possible. X-ray crystallographic analysis of a putative OxDC from *Thermotoga*

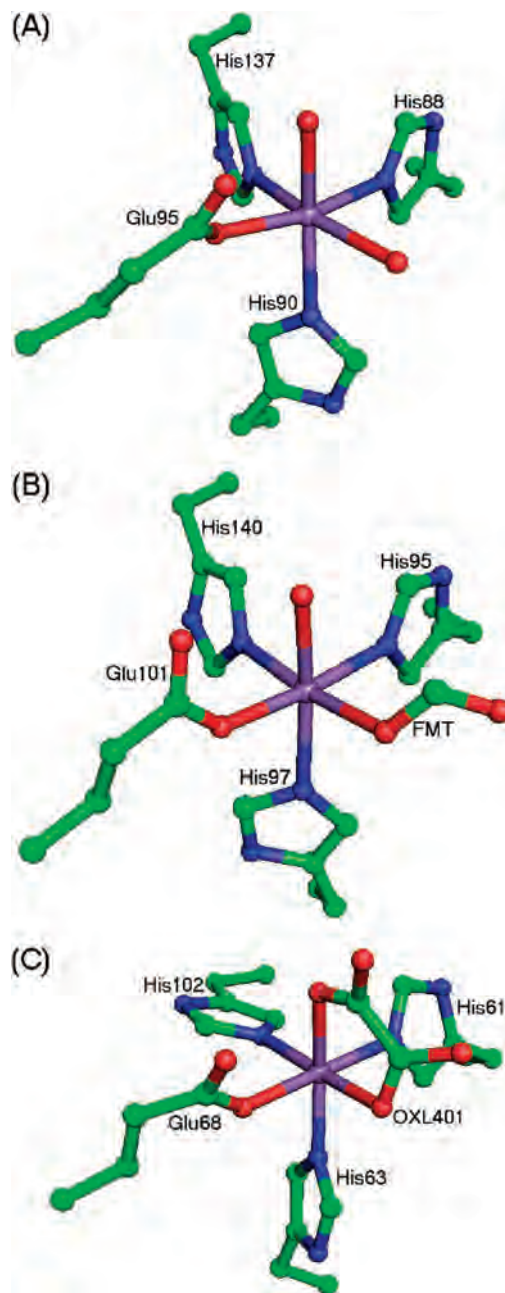


Figure 1. Representation of the active site structures of OxDC and OxOx based on coordinates from PDB files. (A) Manganese binding site in OxOx from *H. vulgare* (pdb 1FI2),¹³ (B) manganese binding site of domain I of OxDC from *B. subtilis* (pdb 1J58, formate complex),¹² and (C) manganese binding site (oxalate complex) of a putative OxDC from *T. maritima* (pdb 1O4T).¹⁴

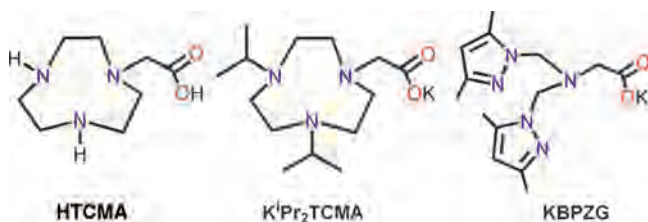
maritima (Figure 1C) revealed the enzyme–substrate interaction by coordination of oxalate to the Mn^{II} ion in a bidentate mode.¹⁴ A very recent study on OxOx, where the substrate analogue glycolate was employed, showed it to be bound in a monodentate fashion to the metal.¹⁵

In addition to the biological interest in understanding the mechanisms of OxOx and OxDC, the development of model complexes for these enzymes is also of great commercial value because of their potential applications in medical diagnosis (e.g., determination of the urinary levels of oxalate),

- (8) Tanner, A.; Bowater, L.; Fairhurst, S. A.; Bonermann, S. *J. Biol. Chem.* **2001**, *276*, 43627–43634.
 (9) Requena, L.; Bornemann, S. *Biochem. J.* **1999**, *343*, 185–190.
 (10) Chang, C. H.; Svedruić, D.; Ozarowski, A.; Walker, L.; Yeagle, G.; Britt, R. D.; Angerhofer, A.; Richards, N. G. *J. Biol. Chem.* **2004**, *279*, 52840–52849.
 (11) Whittaker, M. M.; Whittaker, J. W. *J. Biol. Inorg. Chem.* **2002**, *7*, 136–145.
 (12) Anand, R.; Dorrestein, P. C.; Kinsland, C.; Begley, T. P.; Ealick, S. E. *Biochemistry* **2002**, *41*, 7659–7669.
 (13) Woo, E. J.; Dunwell, J. M.; Goodenough, P. W.; Marvier, A. C.; Pickersgill, R. W. *Nat. Struct. Biol.* **2000**, *7*, 1036–1040.
 (14) Schwarzenbacher, R.; von Delft, F.; Jaroszewski, L.; Abdubek, P.; Ambing, E.; Biorac, T.; Brinen, L. S.; Canaves, J. M.; Cambell, J.; Chiu, H. J. *Proteins* **2004**, *56*, 392–395.
 (15) Opaleye, O.; Rose, R.-S.; Whittaker, M. M.; Woo, E.-J.; Whittaker, J. W.; Pickersgill, R. W. *J. Biol. Chem.* **2006**, *281*, 6428–6433.
 (16) Borowski, T.; Bassan, A.; Richards, N. G. J.; Siegbahn, P. E. P. *J. Chem. Theory Comput.* **2005**, *1*, 686–693.
 (17) Reinhardt, L. A.; Svedruić, D.; Chang, C. H.; Cleland, W. W.; Richards, N. G. *J. Am. Chem. Soc.* **2003**, *125*, 1244–1252.
 (18) Escutia, M. R.; Bowater, L.; Edwards, A.; Bottrill, A. R.; Burrell, M. R.; Polanco, R.; Vicuña, R.; Bornemann, S. *Appl. Environ. Microbiol.* **2005**, *71*, 3608–3616.
 (19) Chang, C. H.; Richards, N. G. *J. Chem. Theory Comput.* **2005**, *1*, 994–1007.
 (20) Muthusamy, M.; Burrell, M. R.; Thorneley, R. N. F.; Bornemann, S. *Biochemistry* **2006**, *45*, 10667–10673.
 (21) Svedruić, D.; Liu, Y.; Reinhardt, L. A.; Wroclawska, E.; Cleland, W. W.; Richards, N. G. *J. Arch. Biochem. Biophys.* **2007**, *464*, 36–47.
 (22) Whittaker, M. M.; Pan, H.-Y.; Yukl, E. T.; Whittaker, J. W. *J. Biol. Chem.* **2007**, *282*, 7011–7023.

- (23) Dunwell, J. M.; Khuri, S.; Gane, P. J. *Microbiol. Mol. Biol. Rev.* **2000**, *64*, 153–179.

Chart 1



in the treatment of disorders related to oxalate, and in bioremediation.²³ In spite of the evident biological and commercial importance in modeling OxDC and OxOx, few examples of claimed model complexes are available in the literature, particularly those recently reported by Berreau and co-workers.^{24–26}

In the last two decades our group has been engaged in designing model complexes of manganese-containing enzymes. Extending our studies we have used N₃O-donor ligands (Chart 1) to synthesize new Mn^{II} complexes, which are presented here and demonstrated to be good structural models for the oxalate metabolizing enzymes. Moreover, complex **2** is proposed as the first structural model for the resting state of the active site of OxOx and OxDC that matches the first coordination spheres well. The compounds were characterized by several techniques including X-ray crystallographic analysis, X-band EPR, electrospray ionization mass spectrometry (ESI-MS), and cyclic voltammetry.

Experimental Section

Abbreviations. OxDC: Oxalate Decarboxylase; OxOx: Oxalate Oxidase; TCMA: TriazaCycloNonaneMonoacetate; TACN: 1,4,7-triazacyclononane; KⁱPr₂TCMA: potassium 1,4-diisopropyl-1,4,7-triazacyclononane-*N*-acetate (KBPZG: potassium *N,N*-bis(3,5-dimethylpyrazolylmethyl)glycinate; IPG: *N*-[(1-methylimidazol-2-yl)methyl]-*N*-(2-pyridylmethyl)glycinate; BIG: *N,N*-bis[(1-methylimidazol-2-yl)methyl]glycinate; TBAClO₄: tetrabutylammonium perchlorate.

Materials and Measurements. The ligands were synthesized as previously described.^{27,28} All of the chemicals used for syntheses and analyses were of analytical grade and used without further purification. Infrared spectra (KBr pellets) were recorded using a Perkin-Elmer Spectrum BX-FTIR spectrometer. Elemental analyses were performed using a Perkin-Elmer 2400 Series II Analyzer. ESI-MS spectra were recorded using a Micromass LCT Time-of-Flight mass spectrometer with Electrospray and APCI, coupled to a Waters 1525 Binary HPLC Pump. Cyclic voltammograms were recorded in methanol solutions using a BAS CV50W potentiostat at room temperature (22 ± 1) °C and under argon atmosphere. A standard three-electrode cell composed by the following electrodes was used: a glassy carbon working, a platinum auxiliary, and a Ag/AgCl reference. TBAClO₄ [0.1M] was used as supporting electrolyte and

the ferrocenium-ferrocene couple²⁹ was employed to monitor the reference electrode potential ($E_{1/2} = 205$ mV vs Ag/AgCl for complexes **1** and **2**, and $E_{1/2} = 366$ mV vs Ag/AgCl for complex **3**). X-band EPR spectra were recorded using a Bruker EMX electron spin resonance spectrometer with a Varian liquid nitrogen cryostat or an Oxford Instruments liquid helium cryostat.

Syntheses. [Mn(TCMA)(H₂O)]CF₃SO₃, Complex 1. A solution of the TCMA·2HCF₃SO₃ ligand (0.51 g, 1 mmol in 5 mL of CH₃OH) was neutralized with NaOCH₃ (0.40 mL, 1 mmol of a 25% solution in CH₃OH) and reacted with MnCl₂·4H₂O (0.20 g, 1 mmol in 2 mL of water) under nitrogen. The reaction mixture was warmed (ca. 50 °C) under nitrogen and stirred for 1 h. The slow evaporation of the solvent under nitrogen flow provided colorless single crystals. FTIR (KBr, cm⁻¹): 3326, 3261 ν(NH); 2930–2870 ν(CH); 1610 ν(C=O); 1568 ν_{asym}(OAc); 1406 ν_{sym}(OAc); 1130–1024 (CF₃SO₃); 1099 ν(C–N). ESI-MS *m/z* (positive mode) (CH₃OH): 273 (100%, [Mn(TCMA)(CH₃OH)]⁺) and 517 (32%, [Mn₂(TCMA)₂(H₂O)(OH)]⁺). Elemental analysis: calcd for MnC₉N₃H₁₈O₆F₃S₃: calcd (found): C, 26.48 (26.50); H, 4.44 (4.05); N, 10.29 (10.46) %. Single crystals suitable for X-ray crystallographic analysis were obtained with both CF₃SO₃⁻ and PF₆⁻ (by addition of NH₄PF₆) anions. Because of the better quality of the data, the crystal structure determination (sections on Crystal Structure Determination and Crystal Structures of Complexes **1–3**) is related to the PF₆⁻ derivative. The remaining analyses were performed using the CF₃SO₃⁻ derivative.

[Mn(ⁱPr₂TCMA)(H₂O)₂]NO₃, Complex 2. Complex **2** was obtained by the addition of a Mn(NO₃)₂·6H₂O solution (0.29 g, 1 mmol in 2 mL of water) to a suspension of the ⁱPr₂TCMA ligand (0.31 g, 1 mmol in 10 mL of CH₃CN) under nitrogen. The reaction mixture was heated (ca. 50 °C) under nitrogen and stirred for about 30 min. Slow evaporation of the solvent under nitrogen flow provided colorless needles suitable for X-ray crystallographic analysis. FTIR (KBr, cm⁻¹): 2972–2850 ν(CH); 1609 ν(C=O); 1384 (NO₃⁻). ESI-MS *m/z* (positive mode) (CH₃OH): 357 (100%, [Mn(ⁱPr₂TCMA)(CH₃OH)]⁺), 325 (75%, [Mn(ⁱPr₂TCMA)]⁺). Elemental analysis: calcd for MnC₁₄N₄H₃₂O₇·3/2H₂O: calcd (found): C, 37.96 (38.26); H, 7.13 (7.07); N, 13.51 (13.56) %.

[Mn(BPZG)(H₂O)]NO₃, Complex 3. Complex **3** was obtained by the same procedure described for complex **2**, employing CH₃OH instead of CH₃CN. Colorless single crystals suitable for X-ray crystallographic analysis were also grown by slow evaporation of the solvent under nitrogen flow. FTIR (KBr, cm⁻¹): 2961–2925 ν(C–H); 1654 ν_{asym}(C=O); 1552, 1465–1422 ν(C=N), ν(C=C); 1383 (NO₃⁻); 1046 ν(C–N). ESI-MS *m/z* (positive mode) (CH₃OH): 377 (100%, [Mn(BPZG)(CH₃OH)]⁺). Elemental analysis: calcd for MnC₁₄N₆H₂₄O₇: calcd (found): C, 37.93 (37.78); H, 5.46 (5.21); N, 18.96 (19.16) %.

Crystal Structure Determination. A crystal of complex **1** was attached to a glass fiber and mounted on a Siemens SMART system for data collection at 173(2) K using Mo Kα radiation (λ = 0.71073 Å). An initial set of cell constants was calculated from reflections harvested from three sets of 20 frames. Final cell constants were calculated from a set of 9967 strong reflections from the data collection. The data were processed with SADABS³⁰ and corrected for absorption. The structure was solved and refined with the

- (24) Grzyska, M. M. M.; Szajna, E.; Shipley, C.; Arif, A. M.; Mitchel, M. H.; Halfen, J. A.; Berreau, L. M. *Inorg. Chem.* **2003**, *42*, 7472–7488.
- (25) Fuller, A. L.; Watkins, R. E.; Dunbar, K. R.; Prosvirin, A. V.; Arif, A. M.; Berreau, L. M. *Dalton Trans.* **2005**, 1891–1896.
- (26) Fuller, A. L.; Watkins, R. E.; Arif, A. M.; Berreau, L. M. *Inorg. Chim. Acta* **2006**, *359*, 1282–1290.
- (27) Scarpellini, M.; Wu, A. J.; Kampf, J. W.; Pecoraro, V. L. *Inorg. Chem.* **2005**, *44*, 5001–5010.
- (28) Odom, D.; Gramer, C. J.; Young, V. G., Jr; Hilderbrand, S. A.; Sherman, S. E. *Inorg. Chim. Acta*, **2000**, *297*, 404–410.

- (29) Gagné, R. R.; Koval, C. A.; Lisensky, G. C. *Inorg. Chem.* **1980**, *19*, 2854–2855.

- (30) Sheldrick, G. M. *SADABS, Program for Empirical Absorption Correction of Area Detector Data*, version 2.10; University of Göttingen: Göttingen, Germany, 2003; Saint Plus, version 7.01, Bruker Analytical X-ray, Madison, WI, 2003.

Table 1. Crystallographic Data for Complexes 1–3

	complex 1	complex 2	complex 3
empirical formula	C ₉ H ₂₂ F ₆ MnN ₃ O ₄ P	C ₁₄ H ₃₂ MnN ₄ O ₇	C ₁₄ H ₂₄ MnN ₆ O ₇
formula weight	436.21	423.38	443.33
temperature (K)	173(2)	123(2)	123(2)
wavelength (Å)	0.71073	0.71073	0.71073
crystal system	orthorhombic	orthorhombic	monoclinic
space group	<i>P</i> 2 ₁ 2 ₁ 2 ₁	<i>P</i> 2 ₁ 2 ₁ 2 ₁	<i>P</i> 2 ₁ / <i>n</i>
unit cell dimensions			
<i>a</i> (Å)/α (°)	8.445(2)/90	9.812(1)/90	13.8976(13)/90
<i>b</i> (Å)/β (°)	13.954(3)/90	13.647(2)/90	9.5576(8)/97.979(4)
<i>c</i> (Å)/γ (°)	14.415(3)/90	14.403(2)/90	14.8122(14)/90
volume (Å ³)	1698.6(6)	1928.5(5)	1948.4(3)
<i>Z</i> /calculated density (mg/m ³)	4/1.706	4/1.458	4/1.511
absorption coefficient (mm ⁻¹)	0.953	0.727	0.727
<i>F</i> (000)	892	900	924
crystal size (mm)	0.62 × 0.28 × 0.02	0.18 × 0.06 × 0.06	0.340 × 0.10 × 0.06
θ range for data collection (°)	2.03 to 25.05	2.83 to 26.41	3.04 to 24.93
limiting indices	−10 ≤ <i>h</i> ≤ 10 −16 ≤ <i>k</i> ≤ 16 −17 ≤ <i>l</i> ≤ 13	−12 ≤ <i>h</i> ≤ 12 −17 ≤ <i>k</i> ≤ 17 −17 ≤ <i>l</i> ≤ 17	−16 ≤ <i>h</i> ≤ 16 −11 ≤ <i>k</i> ≤ 11 −17 ≤ <i>l</i> ≤ 17
reflections collected	10941	17532	32461
reflections unique	2994 [<i>R</i> _{int} = 0.0443]	3947 [<i>R</i> _{int} = 0.0644]	14044 [<i>R</i> _{int} = 0.0000]
absorption correction		semiempirical from equivalents	
max. and min. transmission	0.9812 and 0.5897	0.9577 and 0.8802	0.9577 and 0.7902
refinement method	full-matrix least-squares on <i>F</i> ²		
data/restraints/parameters	2994/2/225	3947/0/255	14044/0/275
goodness-of-fit on <i>F</i> ²	1.039	1.033	1.048
final <i>R</i> indices [<i>I</i> > 2σ(<i>I</i>)]	<i>R</i> ₁ = 0.0394/ <i>wR</i> ₂ = 0.1046	<i>R</i> ₁ = 0.0353/ <i>wR</i> ₂ = 0.0634	<i>R</i> ₁ = 0.0665/ <i>wR</i> ₂ = 0.1660
<i>R</i> indices (all data)	<i>R</i> ₁ = 0.0417/ <i>wR</i> ₂ = 0.1063	<i>R</i> ₁ = 0.0512/ <i>wR</i> ₂ = 0.0683	<i>R</i> ₁ = 0.0960/ <i>wR</i> ₂ = 0.1791
largest diff. peak and hole	0.943 and −0.486 e [−] Å ^{−3}	0.242 and −0.242 e [−] Å ^{−3}	0.654 and −0.600 e [−] Å ^{−3}

Siemens SHELXTL-Plus³¹ (version 5.0) software package. With the exception of the hydrogen atoms on the methanol solvent molecule, all hydrogen atoms were located from the electron density map and refined in ideal positions with isotropic displacement parameters. The placement of the hydrogen atoms on the solvent methanol molecule was determined by the position that maximized the sum of the electron density at the calculated positions.

Crystals of complexes **2** and **3** were mounted on a standard Bruker SMART 1K CCD-based X-ray diffractometer equipped with an LT-2 low temperature device and normal focus Mo-target X-ray tube ($\lambda = 0.71073$ Å) operated at 2000 W power (50 kV, 40 mA). The X-ray intensities were measured at 123(2) K, and the final cell constants (Table 1) were based on the *xyz* centroids of reflections above 10σ(*I*). Analysis of the data showed negligible decay during data collection. Indexing for complex **3** was performed by use of CELL_NOW,³² which indicated that the crystal was a three component nonmerohedral twin. The data were processed with SADABS³⁰ (complex **2**) and TWINABS³³ (complex **3**) and corrected for absorption. The structures were solved and refined with the Bruker SHELXTL³⁴ (version 6.12) software package. All nonhydrogen atoms were refined anisotropically with the hydrogen atoms placed in a combination of idealized and refined positions.

Figures of the molecular structures were produced using the Oak Ridge Thermal Ellipsoid Plot (ORTEP)³⁵ program. Solvent molecules, counterions and hydrogen atoms on ligands have been omitted in the drawings for reasons of clarity. All complexes display hydrogen bond interactions. These data are presented as Supporting Information in Table S1. Additional crystal structure and refinement data for all of the complexes are summarized in Table 1 and given as Supporting Information in a CIF file. Figures of the active sites of the enzymes were generated using PyMOL (<http://pymol.sourceforge.net>).

Results

Crystal Structures of Complexes 1–3. Complex **1** forms colorless crystals belonging to the orthorhombic crystal system, space group *P*2₁2₁2₁. The crystallographic data, and the main bond distances and angles for **1** are presented in Tables 1 and 2, respectively. The structure of complex **1** reveals an infinite chain of Mn^{II} monomeric units that are linked by carboxylate groups in a *syn-antipattern*, in which the Mn–O–C–O–Mn unit is aligned parallel to the axis *a* of the unit cell (Figure 2). Each Mn^{II} is seven-coordinate, distorted pentagonal bipyramidal, with the equatorial plane being composed by two nitrogen (N2 and N5) and three carboxylic oxygen atoms (O2, O1₄, and O2₄). The O2 atom belongs to the carboxylic pendant arm of the same TCMA[−] ligand that provides the nitrogen atoms, whereas the O1₄ and O2₄ are from the TCMA[−] ligand coordinated to the neighboring Mn^{II} center. The axial positions are occupied by a nitrogen atom (N8) and an oxygen atom (O3) from a water molecule. The Mn–N bond distances range from 2.281(3) to 2.358(3) Å. The Mn1–O2₄ (2.56 Å) is the longest Mn–O_{carboxylic} bond distance in the coordination sphere [Mn1–O2: 2.214(2) Å, Mn1–O1₄: 2.241(2) Å]. The Mn⋯Mn distance is 4.67 Å. The similarity of the C–O

(31) SHELXTL-Plus, version 5.0; Siemens Industrial Automation, Inc.: Madison, WI.

(32) Sheldrick, G. M. *CELL_NOW, Program for Indexing Twins and Other Problem Crystals*; University of Göttingen: Göttingen, Germany, 2003.

(33) Sheldrick, G. M. *TWINABS, Program for Empirical Absorption Correction of Area Detector Data*, v. 1.02.; University of Göttingen: Göttingen, Germany, 2003; Saint Plus, v. 7.01, Bruker Analytical X-ray, Madison, WI, 2003.

(34) Sheldrick, G. M. *SHELXTL*, version 6.12; Bruker Analytical X-ray: Madison, WI, 2001.

(35) Farrugia, L. J. *J. Appl. Crystallogr.* **1997**, *30*, 565.

(36) Studer, M.; Riesen, A.; Kaden, T. A. *Helv. Chim. Acta* **1989**, *72*, 307–312.

(37) Graham, B.; Moubaraki, B.; Murray, K. S.; Spiccia, L.; Cashion, J. D.; Hockless, D. C. R. *J. Chem. Soc., Dalton Trans.* **1997**, 887–893.

(38) Just, V. J.; Stevenson, C. E. M.; Bowater, L.; Tanner, D. M.; Lawson, D. M.; Bornemann, S. *J. Biol. Chem.* **2004**, *279*, 19867–19874.

Table 2. Bond Lengths (Å) and Angles (°) for Complexes 1–3

complex 1 ^a		complex 2		complex 3 ^b	
Mn(1)–O(3)	2.181(3)	Mn(1)–O(3)	2.1461(19)	Mn(1)–O(2)	2.093(2)
Mn(1)–O(2)	2.214(2)	Mn(1)–O(4)	2.164(2)	Mn(1)–O(3)	2.158(2)
Mn(1)–O(1)#1	2.241(2)	Mn(1)–O(1)	2.2178(18)	Mn(1)–O(1)	2.111(19)
Mn(1)–N(5)	2.281(3)	Mn(1)–N(1)	2.278(2)	Mn(1)–N(5)	2.224(3)
Mn(1)–N(8)	2.289(3)	Mn(1)–N(3)	2.339(2)	Mn(1)–N(3)	2.257(3)
Mn(1)–N(2)	2.358(3)	Mn(1)–N(2)	2.373(2)	Mn(1)–N(1)	2.417(2)
Mn(1)–O(2)#1	2.558(2)	O(1)–C(1)	1.284(3)	O(1)–C(1)	1.249(4)
O(1)–C(12)	1.266(4)	O(2)–C(1)	1.235(3)	O(2)–C(1)#1	1.272(3)
O(2)–C(12)	1.264(4)			C(1)–O(2)#2	1.272(3)
O(3)–Mn(1)–O(2)	87.11(9)	O(3)–Mn(1)–O(4)	85.49(9)	O(2)–Mn(1)–O(3)	93.21(8)
O(3)–Mn(1)–O(1)#1	99.04(10)	O(3)–Mn(1)–O(1)	97.05(8)	O(2)–Mn(1)–O(1)	85.38(8)
O(2)–Mn(1)–O(1)#1	83.02(9)	O(4)–Mn(1)–O(1)	87.43(7)	O(3)–Mn(1)–O(1)	175.68(9)
O(3)–Mn(1)–N(5)	91.96(11)	O(3)–Mn(1)–N(1)	162.42(9)	O(2)–Mn(1)–N(5)	110.67(9)
O(2)–Mn(1)–N(5)	149.30(10)	O(4)–Mn(1)–N(1)	108.35(9)	O(3)–Mn(1)–N(5)	91.44(9)
O(1)#1–Mn(1)–N(5)	127.28(10)	O(1)–Mn(1)–N(1)	73.45(7)	O(1)–Mn(1)–N(5)	92.88(8)
O(3)–Mn(1)–N(8)	167.24(11)	O(3)–Mn(1)–N(3)	91.71(9)	O(2)–Mn(1)–N(3)	101.52(9)
O(2)–Mn(1)–N(8)	99.36(11)	O(4)–Mn(1)–N(3)	99.36(11) 163.06(8)	O(3)–Mn(1)–N(3)	99.36(11) 92.30(9)
O(1)#1–Mn(1)–N(8)	92.70(10)	O(1)–Mn(1)–N(3)	109.50(7)	O(1)–Mn(1)–N(3)	83.99(8)
N(5)–Mn(1)–N(8)	76.84(11)	N(1)–Mn(1)–N(3)	78.10(8)	N(5)–Mn(1)–N(3)	147.31(9)
O(3)–Mn(1)–N(2)	94.54(11)	O(3)–Mn(1)–N(2)	114.94(8)	O(2)–Mn(1)–N(1)	159.30(8)
O(2)–Mn(1)–N(2)	73.47(9)	O(4)–Mn(1)–N(2)	87.96(8)	O(3)–Mn(1)–N(1)	107.05(9)
O(1)#1–Mn(1)–N(2)	152.16(9)	O(1)–Mn(1)–N(2)	147.18(8)	O(1)–Mn(1)–N(1)	74.10(8)
N(5)–Mn(1)–N(2)	76.02(11)	N(1)–Mn(1)–N(2)	77.28(8)	N(5)–Mn(1)–N(1)	73.83(9)
N(8)–Mn(1)–N(2)	76.98(11)	N(3)–Mn(1)–N(2)	78.07(7)	N(3)–Mn(1)–N(1)	74.03(9)
O(3)–Mn(1)–O(2)#1	78.3(1)			O(1)–C(1)–O(2)#2	125.0(3)
O(2)–Mn(1)–O(2)#1	130.9(1)			O(1)–C(1)–O(2)	119.6(3)
O(1)#1–Mn(1)–O(2)#1	54.3(1)				
N(5)–Mn(1)–O(2)#1	78.5(1)				
N(8)–Mn(1)–O(2)#1	105.0(1)				
N(2)–Mn(1)–O(2)#1	153.3(1)				

^a Symmetry transformations used to generate equivalent atoms. #1: $x + 1/2, -y + 3/2, -z$. #2: $x - 1/2, -y + 3/2, -z$. ^b Symmetry transformations used to generate equivalent atoms. #1: $-x + 3/2, y + 1/2, -z + 3/2$. #2: $-x + 3/2, y - 1/2, -z + 3/2$.

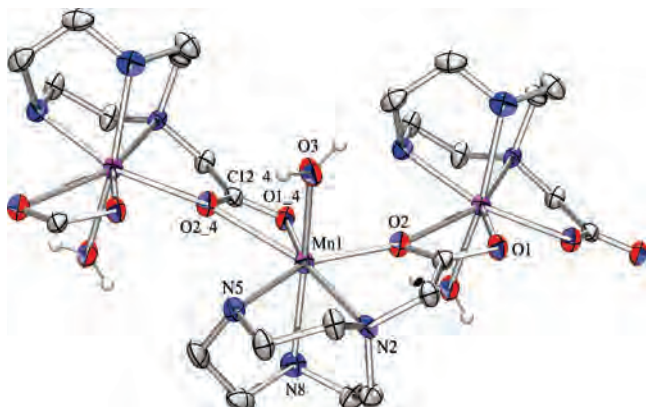


Figure 2. ORTEP³⁵ view of a section containing three subunits of the polymer complex **1**, showing the atoms labeling and the 50% probability ellipsoids.

bond distances [C12–O1_4: 1.266(4) and C12–O2_4: 1.264(4) Å] is consistent with delocalization of the negative charge over the carboxylate-bridging group. The crystallization of **1** as an infinite chain of Mn^{II} complexes linked by the pendant carboxylate arm of the TCMA[−] ligand is similar to structures previously reported for other complexes with the same ligand: [Cu(TCMA)]⁺³⁶ and [Zn(TCMA)(H₂O)]⁺²⁸. However, this behavior is not observed for [Fe(TCMA)Cl₂]³⁷ and [Mg(TCMA)(H₂O)₂]⁺²⁸ complexes that crystallize as mononuclear compounds. In all of these complexes, the three nitrogen atoms of the macrocyclic TCMA[−] ligand coordinate facially. The average of the M–N bond distances in **1** is the longest (2.309 Å) of the series: [Mg(TCMA)(H₂O)₂]⁺²⁸, 2.199

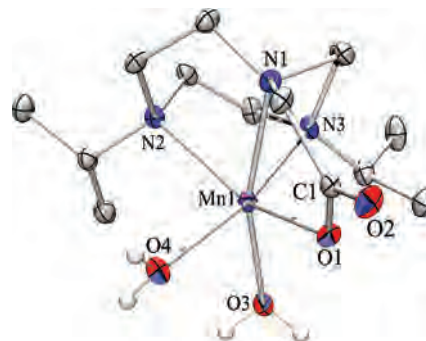


Figure 3. ORTEP³⁵ view of complex **2**, showing the atoms labeling and the 50% probability ellipsoids.

Å; [Fe(TCMA)Cl₂], 2.185 Å; and [Zn(TCMA)(H₂O)]⁺²⁸, 2.177 Å. The M–O_{carboxylic} bond distance of the endogenous carboxylate observed for **1** [2.214(2) Å] is also the longest of the series.

Complex **2** crystallizes as colorless crystals that belong to the orthorhombic crystal system, space group $P2_12_12_1$. The crystallographic data, and the main bond distances and angles for this complex are presented in Tables 1 and 2, respectively. An ORTEP³⁵ representation of complex **2** (Figure 3) shows a mononuclear Mn^{II} cation six-coordinate in a distorted octahedral geometry. In the equatorial plane two nitrogen atoms [N1: 2.278(2) and N3: 2.339(2) Å] from the ⁱPr₂TCMA[−] ligand are coordinated trans to two oxygen atoms [O3: 2.146(2) and O4: 2.164(2) Å] from water molecules. The axial positions are occupied by the atoms N2 [2.373(2) Å] and O1 [2.218(2) Å] from the ⁱPr₂TCMA[−] ligand. In

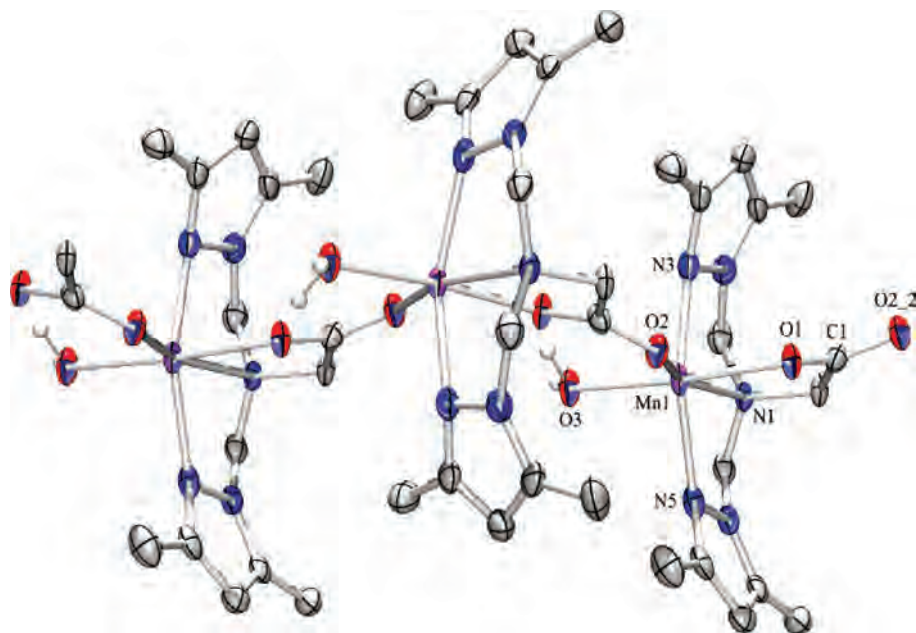


Figure 4. ORTEP³⁵ view of a section containing three subunits of the polymer complex **3**, showing the atoms labeling and the 50% probability ellipsoids.

contrast to those observed for **1**, the C–O bond distances [C1–O1: 1.284(3) and C1–O2: 1.235(3) Å] in complex **2** are nonsymmetrical revealing the carboxyl (C=O) character of the C1–O2 bond. The ⁱPr₂TCMA[−] differs from the TCMA[−] ligand by alkyl residues added onto two nitrogen atoms of the macrocycle (Chart 1). This modification seems to ensure obtaining mononuclear complexes, as observed in **2** and in the Co^{II} analogues [Co(ⁱPr₂TCMA)Cl] and [Co(ⁱPr₂TCMA)(OAc)(H₂O)].²⁷ The three nitrogen atoms of the azamacrocycle coordinate in a facial mode comparable to **1**. According to Table 2, the bond distances between the Mn^{II} center and the isopropyl-substituted nitrogen atoms [N2: 2.373(2) Å and N3: 2.339(2) Å] in **2** are longer than the corresponding bond lengths in **1** [N5: 2.281(3) and N8: 2.289(3) Å].

Complex **3** forms colorless single crystals belonging to the monoclinic crystal system, space group *P*2₁/*n*. The crystallographic data and the main bond distances and angles are presented in Tables 1 and 2, respectively. As observed for **1**, complex **3** crystallizes as an infinite polymeric chain of Mn^{II} complexes as repeat units. Figure 4 is an ORTEP³⁵ representation of a section of the polymer containing three subunits displaying the Mn^{II} ions in a six-coordinate N₃O₃ environment. The nitrogen atoms of the BPZG[−] tripodal ligand coordinate in a meridional mode in such a way that the N_{pyrazole} atoms [N3: 2.257(3) and N5: 2.224(3) Å] are positioned trans to each other. They are part of the equatorial plane, which is completed by an oxygen atom [O3: 2.158(2) Å] from a water molecule coordinated trans to the O1 [2.417(2) Å] carboxylic oxygen atom from the BPZG[−] ligand. The axial positions of the Mn^{II} coordination sphere are occupied by a carboxylic oxygen atom [O3: 2.093(2) Å] and the nitrogen atom of the tertiary amine function [N1: 2.417(2)]. The carboxylate group links the Mn^{II} ions as observed in **1**; however, the C–O bond distances [O1–C1: 1.249(4) and O2–C1#1: 1.272(3) Å] in **3** are nonsymmetri-

cal. Complex **3** represents a different class of compounds than complexes **1** and **2** in the sense that it is coordinated by a tripodal and not by a macrocyclic ligand (Figures 2–4). Moreover, the nitrogen donor atoms originate from pyrazole groups, resembling the electronic structure of the His ligands found in the enzymes.

ESI-MS. To investigate the stability of complexes **1–3** in solution, electrospray ionization mass spectra (ESI-MS, positive mode) of freshly prepared solutions in methanol were recorded. The spectrum of complex **1** shows peaks at *m/z*⁺: 273 (100%) and 517 (32%), which can be formulated, respectively, as the [Mn(TCMA)(CH₃OH)]⁺ and [Mn₂(TCMA)₂(H₂O)(OH)]⁺ species. Complex **3** presents an intricate spectrum with the main peak at 377 (100%) being consistent with the species [Mn(BPZG)(CH₃OH)]⁺. The ESI-mass spectra of complexes **1** and **3** reveal a break of the polymeric structure in solution yielding monomeric Mn^{II} species, which is in agreement with the EPR data (vide infra). The spectrum of complex **2** presents peaks at 357 (100%) and 325 (75%) attributed, respectively, to the species [Mn(ⁱPr₂TCMA)(CH₃OH)]⁺ and [Mn(ⁱPr₂TCMA)]⁺. This result provides evidence for the existence of labile positions on the metal coordination sphere.

EPR Spectroscopy. X-band EPR spectra of complexes **1–3** were recorded from frozen solutions (methanol/toluene 1:1) at liquid nitrogen and helium temperatures and are presented in Figure 5. At 120 K (Figure 5, left) the spectra of **2** and **3** are characterized by six sharp lines centered at *g* ~ 2.0 and by hyperfine coupling constants *A* approximately at 90 × 10^{−4} cm^{−1}. The spectrum of compound **1** exhibits a broader feature overlaying the central lines. At 4.5 K (Figure 5, right) the less intense bands for the forbidden transitions ($\Delta M_s = \pm 1$, $\Delta M_l = \pm 1$) are clearly observed between the sharp six lines (only the spectrum for compound **3** is shown).

Six lines spectra centered at *g* ~ 2.0 (*A* = 90 × 10^{−4} cm^{−1}) have been assigned to allowed transitions ($\Delta M_s = \pm 1$ and

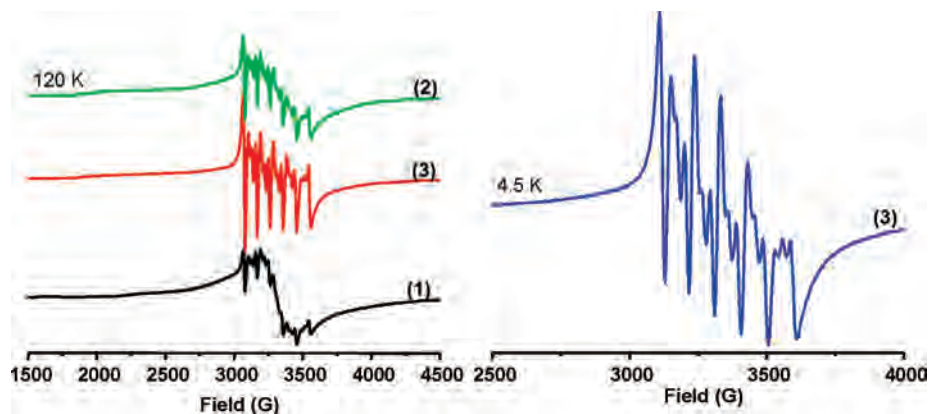


Figure 5. Left panel, X-band EPR spectra of complexes **1–3** in methanol/toluene (1:1) solutions (1×10^{-3} M) at liquid nitrogen temperature. Right panel, X-band EPR of complex **3** in methanol/toluene (1:1) solution (1×10^{-3} M) at 4.5 K. Experimental conditions: microwave frequency, 9.424 GHz; microwave power, 20.2 mW; modulation frequency, 100.0 KHz; modulation amplitude, 10.0 G; receiver gain, 1.0×10^2 ; and conversion time, 40.96 ms.

$\Delta M_I = 0$) in mononuclear ^{55}Mn ($I = 5/2$) centers coordinated octahedrally with oxygen or nitrogen ligands.⁴¹ This type of spectrum is expected for complex **2**, an isolated mononuclear Mn^{II} compound. Nevertheless, for complexes **1** and **3**, the spectra indicate that the chain structures observed in the solid state dissociate into Mn^{II} monomers in solution, probably through interaction with the solvent. At 4.5 K (Figure 5 right panel) additional weak signals, which are assigned to forbidden transitions in Mn^{II} centers, are observed. For complex **1**, the allowed six lines are not as clear as are those of complexes **2** and **3**. In fact, the spectrum of complex **1** in Figure 5 can best be described as an overlay of a broad spectrum typical of a binuclear Mn^{II} species and the six lines characteristic of mononuclear Mn^{II} compounds. Moreover, these results agree quite well with those observed by ESI-MS. The presence of Mn^{II} mononuclear units in solution has also been observed^{39,40} in the analogous manganese complexes with amino-carboxylate ligands, $[\text{Mn}(\text{IPG})(\text{MeOH})_n(\text{PF}_6)_n]$ and $[(\text{BIG})\text{Mn}(\mu\text{-OCO})_2\text{Mn}(\text{BIG})]^{2+}$ which are, respectively, a polymer chain and a binuclear complex in the solid state.

Cyclic Voltammetry. The redox behaviors of complexes **1–3** were investigated by cyclic voltammetry in methanol, under argon, in the potential range +1700 to –1000 mV versus Ag/AgCl. The data were recorded without stirring during the scans and using only freshly prepared solutions. We have not applied a potential for an extended period of time before recording the voltammograms. There was no concentration dependence to the voltammetric response for any of the complexes. The data for complex **2** is shown in Figure 6, and the data for compounds **1** and **3** are provided in the Supporting Information. Complex **1** presents two quasi-reversible processes at $E_{1/2}^1 = 333$ mV ($\Delta E_p = 112$ mV) and $E_{1/2}^2 = 0$ mV ($\Delta E_p = 106$ mV) versus Fc^+/Fc and an additional cathodic peak at $E_{pc} = 120$ mV versus Fc^+/Fc . E^1 can be tentatively attributed

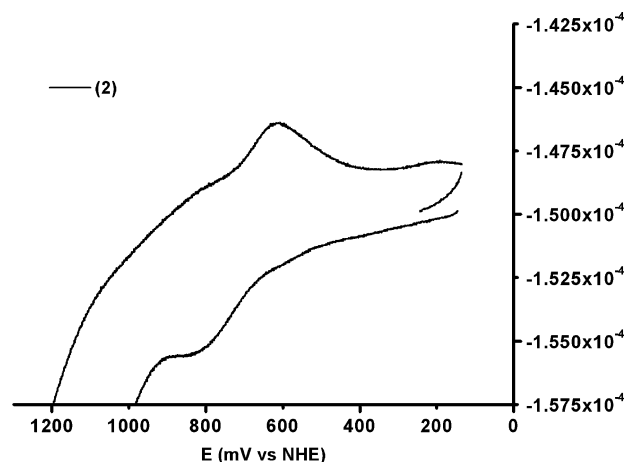


Figure 6. Cyclic voltammogram (CV) of complex **2** in methanol, at room temperature, 0.1 M of TBAClO_4 as the supporting electrolyte. Data were collected using a Ag/AgCl reference electrode, platinum wire auxiliary electrode, glassy carbon working electrode, at scan rate $75 \text{ mV}\cdot\text{s}^{-1}$, $[\text{2}] = 1 \times 10^{-3}$ M. Ferrocene was used as an external standard as described in ref 29. The CV is presented against the Normal Hydrogen Electrode (NHE) to facilitate comparison to the enzymes (using a potential of 0.40 V for Fc^+/Fc vs NHE).

to the $\text{Mn}^{\text{II}} \rightarrow \text{Mn}^{\text{III}}$ process in the mononuclear $[\text{Mn}(\text{TCMA})(\text{CH}_3\text{OH})]^+$ species. The cyclic voltammogram of complex **2** displays a poorly reversible process at $E_{1/2} = 330$ mV versus Fc^+/Fc , (730 mV vs NHE) attributed to the $\text{Mn}^{\text{II}} \rightarrow \text{Mn}^{\text{III}}$ process in the mononuclear species. A second oxidation peak at $E_{pa} = 930$ mV versus Fc^+/Fc (1330 mV vs NHE) can be tentatively assigned to an oxidation process centered on the ligand. Complex **3** exhibits multiple oxidation peaks with the dominant electrochemical waves at $E_{pa}^2 = 727$ mV and $E_{pa}^2 = 1070$ mV versus Fc^+/Fc . These may correspond to the oxidation of two different species in the $\text{Mn}(\text{II})$ oxidation level or the subsequent oxidation of a $\text{Mn}(\text{III})$ species to $\text{Mn}(\text{IV})$. Given the quality of the data, we prefer to refrain from making a specific assignment for each process. Probably, rate-limiting structural changes occur that render all of these processes irreversible or quasi-reversible in the best cases.

Discussion

Although both OxDC and OxOx have been successfully characterized by X-ray crystallography, details about the

(39) Policar, C.; Durot, S.; Lambert, F.; Cesario, M.; Ramiandrasoa, F.; Morgenstern-Badarau, I. *Eur. J. Inorg. Chem.* **2001**, 1807–1818.

(40) Policar, C.; Lambert, F.; Cesario, M.; Morgenstern-Badarau, I. *Eur. J. Inorg. Chem.* **1999**, 2201–2207.

(41) (a) Mabbs, F. E.; Collinson, D. *Studies in Inorganic Chemistry. Electron Paramagnetic Resonance of d Transition Metal Compounds*; Elsevier: Amsterdam, 1992; Vol. 16. (b) Que, L.; Reynolds, M. F. In *Metal Ions in Biological Systems*; Sigel, A., Sigel, H., Eds.; Marcel Dekker: New York, 2000; Vol. 37, pp 505–525.

mechanism of oxalate degradation are still unclear. This leaves much room for speculation on the actual role of manganese in catalysis, the binding mode of the substrate, and, in the case of OxDC which has two manganese binding sites per subunit, the site of activity.^{12,21} Several different pathways, involving all biologically relevant oxidation states of manganese (+II to +IV), have been proposed on the basis of extensive studies of wild-type, recombinant, and mutant enzymes.^{8–10,15–22}

One approach to address these issues is to synthesize small molecule models that very closely mimic the active site of the enzymes. Well characterized models may be a powerful tool to help overcome problems associated with studying the more complex enzymatic systems. To match the donor set found in the active sites of OxOx and OxDC, we employed amino-carboxylate ligands belonging to two different classes (cf. also Chart 1): (1) pyrazole moieties as nitrogen donors to account for the electronic properties of histidine residues and (2) nitrogen containing macrocycles that were shown to provide the correct facial arrangement of N-donors upon coordination.^{28,36} Furthermore, each of the ligands used in this study differ in the degree of steric bulk which can be used to alter the coordination environment about the metal. These modifications lead to solid state structures ranging from infinite chains to monomeric systems which adopt either six- or seven-coordinate environments.

We observe a clear progression from a more crowded, less biomimetic manganese environment to the desired structure as we increase steric bulk on the ligand. Complex **1**, which contains the least sterically hindered ligand (TCMA[−]), crystallized as a polymer with seven-coordinate manganese(II) atoms in the center of each subunit (Figure 2). The TCMA[−] ligand allows for sufficient access to the metal so that both oxygen atoms of the carboxylate group of an adjacent molecule can insert within the Mn(II) coordination sphere. In contrast, the bulky isopropyl groups of the ⁴Pr₂TCMA[−] ligand restrict access of a second carboxylate group to the manganese. The resultant structure, complex **2** (Figure 3), is six-coordinate with the adjacent nonmacrocyclic ligand positions filled with water. Thus, application of steric bulk allows us to realize the desired enzymatic model complex. A more complex system arises with the BPZG[−] ligand as the molecule is no longer a macrocycle but rather a tripodal amine. Furthermore, rather than alkyl amine nitrogen atoms, BPZG[−] utilizes a pyrazole donor. Nonetheless, one can estimate that the N-methyl group of BPZG[−] yields a ligand of intermediary steric bulk between TCMA[−] and ⁴Pr₂TCMA[−]. As a consequence, a six-coordinate structure similar to **2** is obtained; however, rather than being a molecular species, Figure 4 demonstrates that a chain, reminiscent of **1** is isolated. Unlike **1**, **3** has room to accept only one of the carboxylate oxygen atoms of the adjacent molecule. Thus, we observe a series beginning with **1** that is seven-coordinate, with a bidentate carboxylate inserting into the manganese coordination sphere from another molecule, going to a six-coordinate **3**, with a monodentate carboxylate bound from an adjacent molecule, to a truly molecular six-coordinate **2**, with two water ligands filling the coordination sphere.

Despite these solid state structural features, evidence suggests that compounds **1**, **2**, and **3** can dissolve in donor solvents to yield mononuclear Mn(II) complexes. Furthermore, EPR spectroscopy, which is very sensitive to the dimerization of Mn(II), is only consistent with the existence of monomeric Mn(II) species (except for **1**, where the pattern is consistent with the presence of both a binuclear species and a mononuclear species). The sharp six-line pattern and the magnitude of the Mn hyperfine coupling is consistent with the formation of pseudo-octahedral solution species for **2** and **3**. The broader, poorly defined hyperfine signals observed for **1** are consistent with both a seven-coordinate monomer and the presence of a binuclear species when dissolved in water or methanol. Although we assign the solution structure of **3** also as a six-coordinate complex, it differs from that of the TCMA[−] derived **2**.

Because the BPZG[−] ligand is not a macrocycle, it is able to accept either meridional (*mer*-) or facial (*fac*-) coordination modes. We observe in the structure of **3** that the nitrogen atoms form a *mer*- isomer. This observation is in contrast to the related Co(II) compounds²⁷ where the facial arrangement of nitrogen atoms is observed. The Mn(II) coordination sphere is perturbed by the insertion of a carbonylic oxygen atom from a neighboring subunit. This leads to a change in geometry from trigonal-bipyramidal (as seen for Co^{II}) to a distorted octahedron. The polymeric-type structure of **3** has also been observed in the [Mn(IPG)(MeOH)_n(PF₆)_n] complex with the N₃O tripodal ligand IPG: (*N*-[(1-methylimidazol-2-yl)methyl]-*N*-(2-pyridylmethyl)glycinate).^{39,40} It is important to mention that the Mn^{II} complex employing the analogous amino-carboxylate ligand BIG (*N,N*-bis[(1-methylimidazol-2-yl)methyl]glycinate), which differs from BPZG[−] by having two 1-methylimidazole instead of two 3,5-dimethylpyrazole groups, presents a binuclear structure of seven-coordinate Mn^{II} centers.³⁹ The occurrence of polynuclear complexes with these tripodal ligands may be due to the adopted meridional coordination mode, which favors the interaction of the carboxylate group with the neighboring metal center. However, our EPR studies definitively exclude the formation of Mn(II) dimers upon dissolution of **3**. Unfortunately, neither mass spectrometry nor X-band EPR spectroscopy are sufficiently sensitive to distinguish the *mer*- and *fac*- isomers in this system; therefore, we can not definitively assign a solution structure for **3**. However, we feel that the meridional isomer is retained and that the best formulation of **3** in solution is that of the *mer*-diaqua BPZG[−] complex.

Although this arrangement of the nitrogen donor atoms is not consistent with the enzymatic geometry (meridional vs facial, Figure 7), the exogenous carboxylate arm can be considered a model for the monodentate bound substrate oxalate, as observed in the crystal structure of OxOx with the analogue glycolate.¹⁵ This configuration mimics equally well the product of the OxDC reaction (formate) bound to the metal center (Figure 7).^{12,15} Complex **3** thus can be viewed as a model for the interaction between the active site and the product/substrate in the respective enzyme.

(42) XSHHELL, SHELXTL, version 5.1; Bruker Analytical X-ray; Madison, WI, 1998.

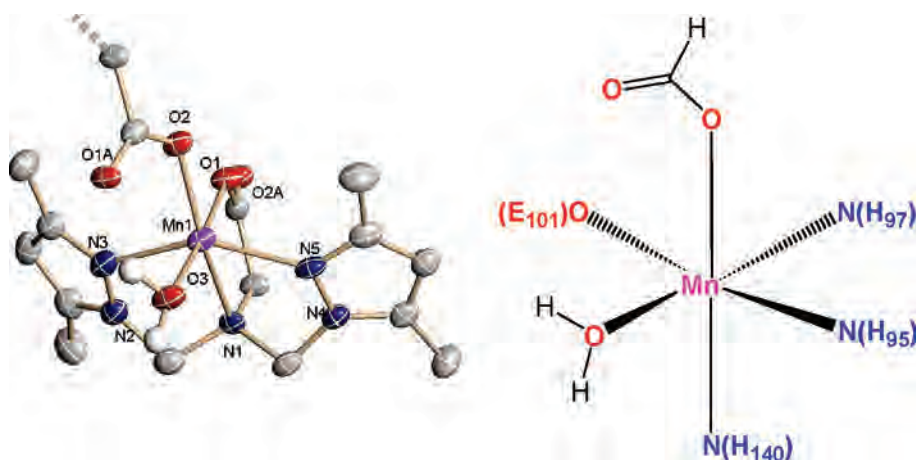


Figure 7. XSEHELL⁴² drawing, showing one subunit of the polymeric [Mn(BPZG)(H₂O)](NO₃), **3** (left), and a sketch of the active site of OxDC with formate bound to Mn in domain I (right, pdb 1L3J).¹²

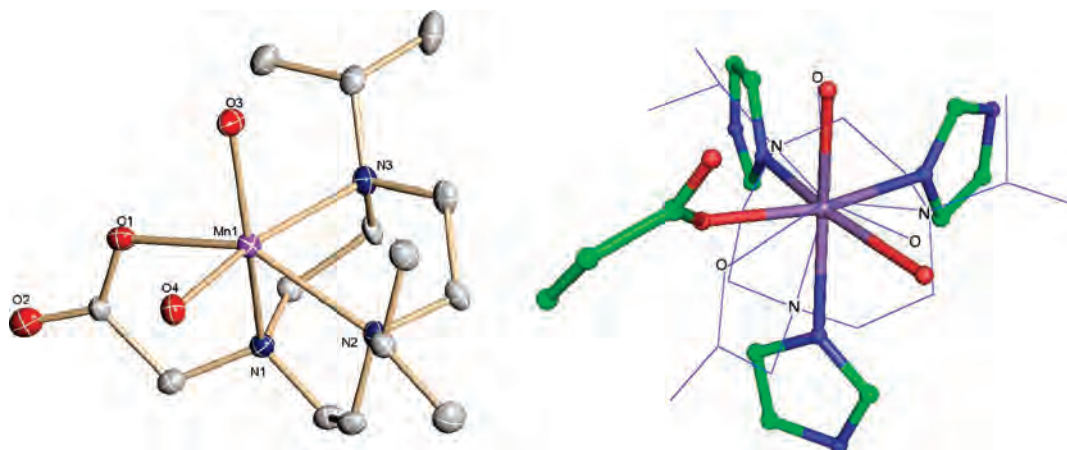


Figure 8. Comparison of the coordination environment in **2** (left) and overlaid with the Mn binding site II in OxDC, pdb 1UW8 (right).³⁸

An even more informative comparison with the enzyme can be achieved with **2**, which was identified to be a facially coordinated monomer in the solid state. The manganese center is coordinated octahedrally by three nitrogen atoms and one carboxylic oxygen atom provided by the macrocyclic ligand scaffold and two oxygen atoms originating from two molecules of water (Figure 4). By comparing the coordination environment of Mn^{II} in complex **2** with that found in OxDC from *B. subtilis*,³⁸ it can be clearly seen that we have synthesized a highly accurate model of the donor set and the coordination geometry found in the active sites of the natural enzymes (Figure 8). The ⁱPrTCMA⁻ ligand provides the exact *fac*- arrangement of nitrogen atoms found both in OxOx as well as in OxDC. Moreover, complex **2** crystallized with two molecules of water *cis* to each other. These are considered as being labile ligands because replacement by other coordinating solvent molecules was observed, for example, in ESI-MS experiments. This feature is important as in the resting state of the oxalate metabolizing enzymes two water molecules are coordinated to the active site Mn^{II}, and they are thought to be replaced by the oxalate anion and dioxygen during the catalytic process. The bond distances around the Mn^{II} center observed in **2** [Mn–N_{av}: 2.33 Å, Mn–O_{carboxylic}: 2.218(2) Å] are slightly longer than those reported for the active site of OxDC [Mn–N_{av}: 2.27 Å,

Mn–O_{carboxylic}: 2.04 Å]³⁸ with the exception of the water molecules. These may be bound more tightly to the Mn center in the complex (Mn–O_{water av}: 2.155 Å in **2**) than in the enzyme (Mn–O_{water av}: 2.35 Å). However, the differences in distances between the model and the protein are probably within the experimental errors given the difficulties with determining ligand distances on metals even in high resolution protein crystal structures. In fact, the metrical values from **2** may be more representative of the actual distances in the enzyme. To the best of our knowledge, compound **2** is the first corroborative structural model for the inner coordination sphere of manganese in these important enzymes.

In addition to the structural studies discussed above, we have carried out a thorough characterization of our complexes to assess their potential not only for acting as structural models but also to elucidate the mechanisms of oxalate metabolism in OxOx and OxDC.^{10,15–22} Whereas determination of redox potentials for proteins is sometimes difficult, especially for intermediate enzyme forms, small molecule redox potentials are often directly accessible. The most recent mechanistic proposals invoke Mn(II) in the resting state of both OxOx and OxDC, whereas Mn(III) is assumed to be the active oxidation level.^{21,22} To gain further insight into the reaction mechanism it is useful to know the Mn^{III/II} reduction potential; however, no experimental data are

available for the enzymatic systems. A step forward has been made by Whittaker and co-workers who, very recently, assigned a range for the reduction potential of the OxOx ($E^0(\text{Mn}^{\text{III/II}}) = +0.4$ to $+1.0$ vs NHE) based on calculations of the free energy change for the oxidative cleavage of oxalate.²²

Unfortunately, it is often difficult to obtain precise reduction potentials for $\text{Mn}^{\text{III/II}}$ because the Mn^{III} oxidation level is unstable because of Jahn–Teller distortions that lead to irreversible electrochemical behavior. As shown in Figure 6 and in the Supporting Information Figure S1, such is the case for complexes **1–3**. Nonetheless, we can place an approximate range on the potential for **2**, which is the relevant species of interest. Ligand oxidation occurs at potentials greater than 1.2 V versus NHE. We observe a quasi-reversible, one electron wave at approximately 700–750 mV versus NHE. Of course, enzyme active sites include features such as selective hydrogen bonding, control of local dielectric, and substrate access that mediate catalysis. However, our data are consistent with the estimates of Whittaker for the potential of this site.²² We have been unable to obtain manganese/oxalate complexes from a stoichiometric reaction between the manganese precursor complexes **1**, **2**, and **3** and the oxalate; however, further studies are underway in our laboratories to examine the complexation of **1–3** with oxalate and related molecules that model possible substrates and reaction products. Nonetheless, the close structural agreement with the active site of the oxalate enzymes that we have achieved, especially with compound **2**, suggests that we have made considerable progress toward the development of functional models for the oxalate metabolizing enzymes.

Conclusion

In summary, we have synthesized and characterized three new Mn^{II} complexes (**1–3**), which are demonstrated to be

excellent corroborative structural model complexes for the active sites of OxOx and OxDC. While complexes **1** and **3** exist as polymers in the solid state, exhibiting the correct donor set, complex **2** is present as a monomeric Mn^{II} compound both in the solid state and in solution. This compound contains two solvent molecules that are likely to be easily displaced, as is proposed in the initial steps of the mechanism outlined for the breakdown of oxalate performed by OxOx and OxDC. These studies have allowed us, using a precise structural model, to establish a range of potentials for the resting state of the enzymes. Our range is in excellent agreement with values predicted using thermochemical calculations.

Acknowledgment. The authors are grateful for grant (GM39406) provided by the National Institutes of Health for support of this research. J.G. would like to thank the Alexander von Humboldt-Foundation for a Feodor Lynen Research-Fellowship. O.J.M. would like to thank the New College Foundation and the New College Alumnae/i Association for support of her research. The authors also acknowledge Carrie Buss, Victor G. Young, Jr., the X-Ray Crystallographic Laboratory for the data collection and structure solution of complex **1** that were conducted at the X-Ray Crystallographic Laboratory, 160 Kolthoff Hall, Chemistry Department, The University of Minnesota, and Ms. Amy Wu for preparation of the HBPZG ligand.

Supporting Information Available: Crystallographic data in CIF format, a table with hydrogen bonds for all complexes, and cyclic voltammograms for **1–3** (PDF). This material is available free of charge via the Internet at <http://pubs.acs.org>.

IC701953G